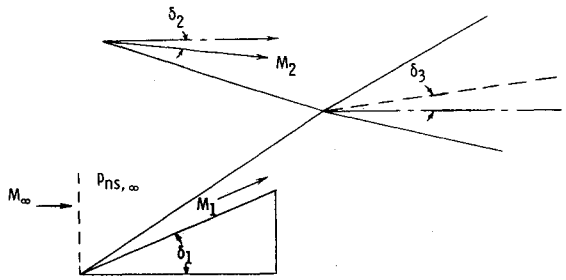

a) Type of interaction calculated.

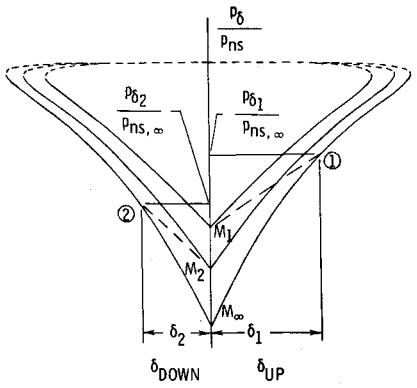

b) Parts of "Logarithmic-Shock-Polar" used.

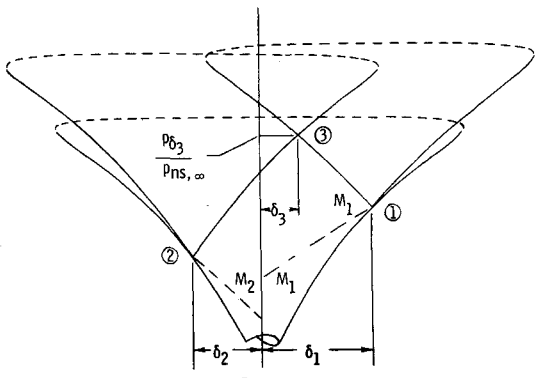

c) Values of $\frac{p_{\delta_3}}{p_{ns,\infty}}$ and δ_3 obtained.

Fig. 2 Example of use of logarithmic-shock-polar diagram.

$$\left(\frac{P_\infty}{P_{ns,\infty}}\right)\left(\frac{\frac{P_1}{P_{ns,\infty}}}{\frac{P_\infty}{P_{ns,\infty}}}\right)\left(\frac{\frac{P_2}{P_{ns,\infty}}}{\frac{P_1}{P_{ns,\infty}}}\right)=\left(\frac{P_\infty}{P_{ns,\infty}}\right)\left(\frac{P_1}{P_\infty}\right)\left(\frac{P_2}{P_1}\right)=\left(\frac{P_2}{P_{ns,\infty}}\right)$$

The value of the logarithmic-shock-polar diagram has been illustrated by its use in two examples, one of which could have necessitated the use of iteration, and one which did not. It can be further utilized to evaluate the two types of three-shock-configuration[2] encountered in shock interaction, i.e., weak oblique wave striking a strong shock, and a weak oblique wave striking another oblique wave of the same family. Both of these have the necessary contact discontinuity line,[2] the first in the form of a shear layer, and the second in the form of an expansion wave. The logarithmic-shock-polar family can be used to estimate the results of reflections from shock waves and expansion waves from a solid wall, or from a free shear layer. These represent all the uses of shock interaction at a point necessary to explain any of Edney's six distinct types of shock

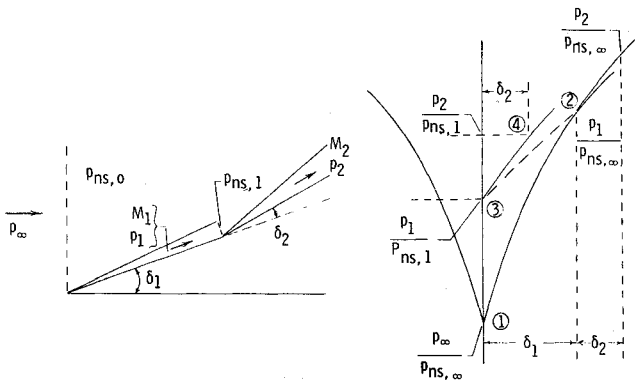

a) Flow over double wedge. b) "Logarithmic-Shock-Polar" for flow over double wedge.

Fig. 3 Another use of logarithmic-shock-polar diagram.

interference pattern. Thus, the pressure-deflection-shock-polar presented in a semilogarithmic format becomes an effective design tool, uniquely applicable to the estimation of multiple shock interference patterns and the resulting pressure changes on affected surfaces.

References

[1] Keyes, J. W. and Hains, F. D., "Analytic and Experimental Studies of Shock Interference Heating in Hypersonic Flows," TN D7139, 1973, NASA.

[2] Courant, R. and Friedrichs, K. O., *Supersonic Flow and Shock Waves*, Interscience Publishers, New York, 1948.

[3] Shapiro, A. H., *The Dynamics and Thermodynamics of Compressible Fluid Flow*, Ronald Press, New York, 1953.

[4] Edney, B. E., "Anomalous Heat Transfer and Pressure Distribution on Blunt Bodies at Hypersonic Speeds in the Presence of an Impinging Shock," FFA Rept. 115, Feb. 1968, The Aeronautical Institute of Sweden, Sweden.

[5] Edney, B. E., Keyes, J. W., Bramlette, T. T., Ives, J., and Hains, F. D., "Theoretical and Experimental Studies of Shock Interference Heating," Rept. 9500-920-195, Oct. 1970, Bell Aerospace Co., Buffalo, N.Y.

[6] Edney, B. E., "Shock Interference Heating and the Space Shuttle," TM X-52876, Vol. 1, July 15–17, 1970, NASA.

[7] "Equations, Tables, and Charts for Compressible Flow," Rept 1135, 1953, NACA.

Calculation of Turbulent Boundary-Layer Shock-Wave Interaction

DAVID C. WILCOX*
Applied Theory Inc., Los Angeles, Calif.

IN the past few years phenomenological turbulence model equations have been applied to increasingly more difficult turbulent flowfield problems. Most complex fields can be solved

Received May 29, 1973. J. G. Trulio of Applied Theory Inc. and P. G. Saffman of the California Institute of Technology provided valuable guidance and assistance during the course of this study. Research was sponsored by the Air Force Aerospace Research Laboratories, Air Force Systems Command, United States Air Force, Contract F33615-72-C-1780.

Index categories: Boundary Layers and Convective Heat Transfer—Turbulent; Jets, Wakes and Viscid-Inviscid Flow Interactions.

* Staff Scientist; presently affiliated with DCW Industries, Sherman Oaks, Calif. Member AIAA.

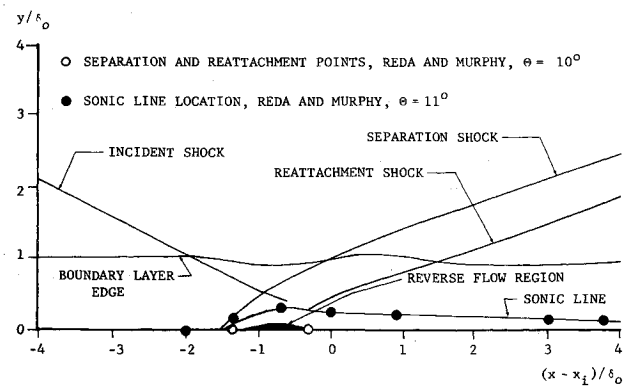

Fig. 1 Computed flowfield structure for the interaction of an oblique shock wave with a turbulent flat plate boundary layer; $M_\infty = 2.96$, $\Theta = 9.87°$.

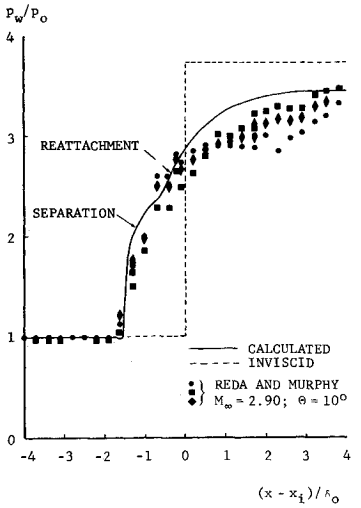

Fig. 3 Comparison of calculated surface pressure distribution with experimental data; $M_\infty = 2.96$; $\Theta = 9.87°$; $Re_{\delta_0} = 2.49 \times 10^5$.

only by numerical means and some progress in obtaining numerical solutions for turbulent flows has been made. The purpose of this Note is to report the recent application of a two parameter turbulence modeling scheme in a finite difference solution to the problem of shock-induced turbulent boundary-layer separation.

Computation was performed with a computer code called AFTON 2PT[1,2] which effects integration of the Saffman turbulence model equations[3,4] for plane transient two-dimensional turbulent fluid motion, by time-marching finite difference methods. The problem addressed was that of oblique incidence of a shock wave, which deflects freestream flow through an angle of 9.87°, on a turbulent boundary layer above an adiabatic flat plate in a Mach 2.96 airstream. Reynolds number based on distance from the plate leading edge was 1.8×10^7 in the vicinity of the interaction region. The shock deflection angle Θ of 9.87° yields an inviscid static pressure rise equivalent to that caused by flow, at the same freestream conditions, into a compression corner with a 20° ramp angle.

The flowfield was computed in two steps: a relatively crude finite difference mesh was used at first and then a finer (higher-mesh-point-density) mesh. As a result of computation with the crude mesh, the boundary layer remained attached to the plate, although the boundary-layer fluid decelerated significantly. The absence of separation was plausible since the flow deflection angle for incipient separation has been found by experimental means[5-7] to lie between 8.5° and 10.5°; hence, the prescribed deflection angle of 9.87° is very close to the "critical deflection angle," or "angle of incipient separation."

Since the deflection angle was so nearly critical for the system in question, there was a strong possibility that discretization errors, particularly near the plate surface, masked a very small domain of separated flow. The density of mesh points was therefore increased sufficiently in the boundary-layer interaction region to resolve a separation bubble whose length would be of the order of one boundary-layer thickness δ_0. Specifically, since turbulent separation bubbles tend to be long and thin, a maximum height of about $0.05\delta_0$ (the height above the plate of the nearest crude-mesh point) was anticipated; in the refined mesh the lowest-lying point was therefore placed at a height of $0.02\delta_0$ above the plate.

Computation with the refined mesh did indeed reveal the presence of a separation bubble which was too small to have been resolved by the crude mesh.

A schematic of the numerical flowfield is shown in Fig. 1. The variable x_i denotes the value of x (x = distance from plate leading edge) at which the incident shock would intersect the plate if no boundary layer were present. The predicted structure of the field is consistent with experimental observation as can be seen by comparing the principal predicted flow regions with those observed for separated and nonseparated fields (see Fig. 2). Figure 1 shows that the incident shock at first compresses the calculated boundary layer, reducing its width to about the same extent as in the case of nonseparated interaction (Fig. 2). The boundary layer then begins to thicken; at the same time a dual reflected-shock pattern develops as a result of the displacement effect of the separation bubble, just as for fully-separated flow (Fig. 2). Hence, as is consistent with the marginal value of the shock deflection angle, the AFTON-computed flowfield displays structural features characteristic of both separated and nonseparated interaction.

Quantitative comparisons of calculated flowfield structure were made with experimental data[6] for very nearly the same flow conditions as those of the computed field. For example, the size, shape and location of the separation bubble were compared with corresponding data for a freestream flow deflection angle of 10°, and the computed sonic line was examined relative to the line measured for a slightly higher flow deflection of 11°. The calculated bubble length of $0.91\delta_0$ (where δ_0 is the boundary-layer thickness just upstream of the interaction region) lies within 10% of the measured bubble length; experimentally-determined separation and reattachment points are shown as open symbols in Fig. 1. Although no data were available with which to compare the height of the calculated region of reverse flow ($0.08\delta_0$), the zero-horizontal-velocity contour was observed to be very thin near its leading edge and considerably thicker near its mid-section—a shape very similar to that observed by Bogdonoff and Kepler.[7]

The computed location of the sonic line is nearly identical to the measured position; experimentally-determined data points defining sonic-line location are shown as closed symbols in Fig. 1. As in the experimental flowfield, the computed sonic line remained relatively far from the plate surface for several boundary-layer thicknesses downstream of the reattachment point. The only significant discrepancy between measured and computed sonic line locations occurred upstream of the separa-

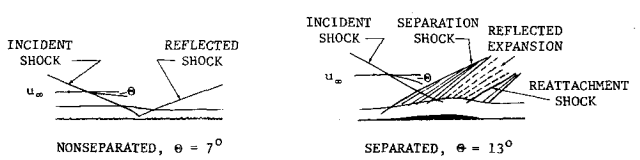

Fig. 2 Observed flowfield structure for the interaction of an oblique shock wave with a turbulent flat plate boundary layer.

tion bubble; the computed sonic line did not extend as far upstream as the measured sonic line. The discrepancy is probably caused by the presence of a larger separation bubble in the experimental field, as is consistent with the higher experimental freestream flow deflection angle of 11°.

Numerical and experimental surface-pressure distributions are shown in Fig. 3 (the experimental flow deflection angle was 10°). It can be seen that AFTON-computed surface pressures fall within the scatter of experimental data and display several significant features of the observed flow, namely: 1) Inflection points of the pressure distribution are found downstream of the steep initial pressure rise. 2) The computed separation point occurs where the ratio of surface to freestream pressure, p_w/p_0, is 2.07, a value within 8% of that measured. 3) The calculated value of p_w/p_0 of 2.63 at the reattachment point differs by less than 5% from the corresponding experimental ratio. 4) The computed and measured pressures approach a common limit with increasing downstream distance from the point of reattachment; the corresponding inviscid limit is higher than in the viscous case at hand.

As in all past Saffman-model applications, no adjustment of the universal constants appearing in the model has been made to force agreement with experimental data. Results obtained indicate that, with no adjustable parameters, the Saffman turbulence model provides an accurate description of flow structure for shock-induced turbulent boundary-layer separation.

References

[1] Trulio, J. G. and Walitt, L., "Numerical Calculations of Viscous Compressible Fluid Flow Around a Stationary Cylinder," CR-1465, 1970, NASA.

[2] Trulio, J. G., Walitt, L., and Niles, W. J., "Numerical Calculations of Viscous Compressible Fluid Flow Over a Flat Plate and Step Geometry," CR-1466, 1970, NASA.

[3] Saffman, P. G., "A Model for Inhomogeneous Turbulent Flow," *Proceedings of the Royal Society*, London, Vol. A317, 1970, pp. 417–433.

[4] Wilcox, D. C. and Alber, I. E., "A Turbulence Model for High Speed Flows," *Proceedings of the 1972 Heat Transfer and Fluid Mechanics Institute*, 1972, pp. 231–252.

[5] Schlichting, H., *Boundary Layer Theory*, 4th ed., McGraw-Hill, New York, 1960, p. 367.

[6] Reda, D. C. and Murphy, J. D., "Shock Wave/Turbulent Boundary-Layer Interactions in Rectangular Channels," *AIAA Journal*, Vol. 11, No. 2, Feb. 1973, pp. 139–140.

[7] Bogdonoff, S. M. and Kepler, C. E., "Separation of a Supersonic Turbulent Boundary Layer," *Journal of Aeronautical Science*, Vol. 22, 1955, pp. 414–424.

Reynolds Stress Measurements in a Hypersonic Boundary Layer

A. DEMETRIADES* AND A. J. LADERMAN†

Philco-Ford Corporation, Newport Beach, Calif.

Introduction

THE steady-state momentum equation for the turbulent boundary layer contains contributions from the flow fluctuations which can be expressed as

$$(\partial/\partial y)(\bar{\rho}\cdot\overline{u'v'}+\bar{u}\cdot\overline{\rho'v'})$$

where the mean velocity $\bar{u}$ and the fluctuation u' are aligned with the surface, ρ' is the fluctuation around the mean density $\bar{\rho}$, and v' is the transverse velocity fluctuation aligned with the direction y normal to the surface.

Since ρ' is of the order of $(\gamma-1)M^2u'$, at low speeds, where the local Mach number approaches zero, the term $\overline{\rho'v'}$ is justifiably neglected in favor of the "Reynolds stress" $\overline{u'v'}$. By the same token, however, the importance of these two terms is reversed in hypersonic boundary layers. A long-needed demonstration of the usefulness of the hot-wire anemometer in providing quantitative turbulence data in hypersonic, compressible boundary layers has been provided recently in Ref. 1. Based on the skills developed in that investigation, the classical X-array hot-wire probe technique has been extended to the measurement of the components $\overline{u'v'}$ and $\overline{\rho'v'}$ of the Reynolds stress. The present Note describes the results obtained from this study.

Theory of X-Probe Response in Compressible Flow

The theory of the X-probe response in compressible flow, including allowances for pressure fluctuations p', has been described in detail in Ref. 2. The resulting equations and their subsequent manipulations to extract the shear stress terms are very complex, and are briefly summarized below for the simplest limit of $p' = 0$. In this case, the instantaneous response of hot-wires 1 and 2 of the X-probe is given by

$$e_i(t) = e_{\tau i}[u(t)+v(t)\cot\phi_i]+e_{\sigma i}\theta(t); \quad i = 1 \text{ and } 2 \tag{1}$$

where ϕ_i is the angle formed by the wire and the mean flow velocity vector, $e_i(t)$ is the normalized voltage fluctuation, $e_{\tau i}$ is the usual hot-wire sensitivity to velocity fluctuations in compressible flow, and $e_{\sigma i}$ is the corresponding sensitivity to static temperature fluctuations. $u(t)$ stands for $u'(t)/\bar{u}$, the local instantaneous velocity fluctuation divided by the mean, and $v(t)$ and $\theta(t)$ are defined in a similar manner. As usual, a third relation is supplied by the correlation $e_1(t)e_2(t)$ of the hot-wire signals. After some algebra these expressions can be put in the familiar form[3,4] involving the modal variables X and Y:

$$Y_1^2 \equiv [\overline{e_1/e_{\sigma 1}}]^2 = A_1X_1^2+A_2X_1+A_3 \tag{2}$$

$$Y_2^2 \equiv [\overline{e_2/e_{\sigma 2}}]^2 = B_1X_2^2+B_2X_2+B_3 \tag{3}$$

$$Z \equiv \overline{e_1e_2}/e_{\sigma_1}e_{\sigma_2} = X_1(X_2C_1+C_2)+X_2D_2+D_3 \tag{4}$$

where

$$X_1 \equiv e_{\tau_1}/e_{\sigma_1}, \qquad X_2 \equiv e_{\tau_2}/e_{\sigma 2}$$

and

$$A_1 = \overline{u^2}+\cot^2\phi_1\,\overline{v^2}+2\cot\phi_1\,\overline{uv} \tag{5a}$$

$$B_1 = \overline{u^2}+\cot^2\phi_2\,\overline{v^2}+2\cot\phi_2\,\overline{uv} \tag{5b}$$

$$C_1 = \overline{u^2}+\cot\phi_1\cot\phi_2\,\overline{v^2}+(\cot\phi_1+\cot\phi_2)\,\overline{uv} \tag{5c}$$

$$A_2 = C_2 = \overline{u\theta}+\cot\phi_1\,\overline{v\theta} \tag{6a}$$

$$B_2 = D_2 = \overline{u\theta}+\cot\phi_2\,\overline{v\theta} \tag{6b}$$

$$A_3 = B_3 = D_3 = \overline{\theta^2} \tag{7}$$

Equations (2) and (3) can be solved for the A_i's and B_i's by operating each hot-wire at a minimum of three overheat currents as usual. Similarly, Eq. (4) can be solved for C_i and D_i by using the method of Ref. 4. To improve the accuracy of these operations in the present experiment, the first wire ($\phi_1 \simeq 45°$) was operated at a total of 15 overheat currents, i_1, while wire no. 2 ($\phi_2 \simeq 135°$) was operated at 5 currents, each of which was held constant while i_1 was varied three times; the coefficients of the resulting overdetermined set of equations were determined by the method of least squares.

The Experiment

The experiment was performed in the turbulent boundary layer

Received June 4, 1973. This work was supported by the U.S. Air Force Space and Missile Systems Organization under Contract F04701-71-C-0035.

Index categories: Boundary Layers and Convective Heat Transfer—Turbulent; Jets, Wakes, and Viscid-Inviscid Flow Interactions.

* Supervisor, Fluid Mechanics Section. Associate Fellow AIAA.

† Principal Scientist, Fluid Mechanics Section. Member AIAA.